The Meteoritical Society

Meteoritics & Planetary Science 43, Nr 12, 2049–2057 (2008)
Abstract available online at http://meteoritics.org

Constraints on central uplift structure from the Manicouagan impact crater

John G. SPRAY* and Lucy M. THOMPSON

Planetary and Space Science Centre, University of New Brunswick, Fredericton, NB E3B 5A3, Canada
*Corresponding author. E-mail: jgs@unb.ca

(Received 26 March 2008; revision accepted 30 October 2008)

Abstract–Recent drilling operations at the 90 km diameter, late Triassic Manicouagan impact crater of Quebec, Canada, have provided new insight into the internal structure of a complex crater's central region. Previous work had indicated that the impact event generated a ~55 km diameter sheet of molten rock of relatively consistent (originally ~400 m) thickness (Floran et al. 1978). The drilling data reveals melt sheet thicknesses of up to ~1500 m, with kilometer-scale lateral and substantial vertical variations in the geometry of the crater floor beneath the melt sheet. The thickest melt section occurs in a 1500 m deep central trough encircled by a horseshoe-shaped uplift of Precambrian basement. The uplift constitutes a modified central peak structure, at least part of which breached the melt sheet. Mineralogical and compositional segregation (differentiation) of the thicker melt sheet section, coupled with a lack of fractionation in the thinner units, shows that the footwall geometry and associated trough structure were in place prior to melt sheet solidification. Marked lateral changes in sub-melt sheet (basement) relief support the existence of a castellated footwall that was created by high-angle, impact-related offsets of 100s to 1000s of meters. This indicates that deformation during the modification stage of the cratering process was primarily facilitated by large-displacement fault systems. This work suggests that Manicouagan is a central peak basin with rings, which does not appear to fit with current complex crater classification schemes.

INTRODUCTION

The hypervelocity impact of meteorites and comets with planetary surfaces imposes very large strains on target materials. Deformation in rocky bodies may be accommodated by hydrodynamic behavior, plastic deformation, fracturing and faulting. The larger impact structures (>3 km diameter on Earth) develop central uplifts and crater margin slumps during the modification stage of the cratering process. This entails the geologically rapid displacement of megatons of rock. The exact mode of deformation of solid materials in response to the hypervelocity collision of meteorites and comets with planetary surfaces is not fully understood. The higher shock pressures generated by projectile impact (>100 GPa) result in melt, vapor and even plasma formation, which contribute to the formation of surface bodies of molten rock and ejecta (e.g., French 1998; Crawford and Schultz 1999; Dressler and Reimold 2001). At lower pressures, below the bulk melting threshold (<60 GPa), the target materials undergo partial melting, various solid-state transformations and footwall displacements involving kilometers of movement. The mechanisms by which very large volumes of rock (thousands to millions of km^3) move during the excavation and gravity-driven modification stages of the impact process remain a subject of debate.

In the larger (complex) impact structures, the end product can include formation of central peaks or ring-shaped uplifts (peak-rings) comprising basement rocks that rise through the impact-generated melt. These tectonic adjustments occur in response to the creation of a bowl-shaped cavity in the target by the projectile and its transferred kinetic energy. The virtually instantaneous formation of a cavity in a planet's crust induces gravitational instabilities, resulting in side wall collapse (slumping), and the elevation of the crater's center as exhumed deeper level material decompresses and adjusts to new stress fields. Several critical questions arise: how is isostatic re-equilibration achieved and at what speed does it take place? Does it occur by bulk flow or localized slip via faulting, or by a combination of the two? Here we present evidence from the ~90 km diameter Manicouagan impact structure of Canada that places constraints on the mechanisms, rates and relative timing of crustal adjustment in the central part of the crater.

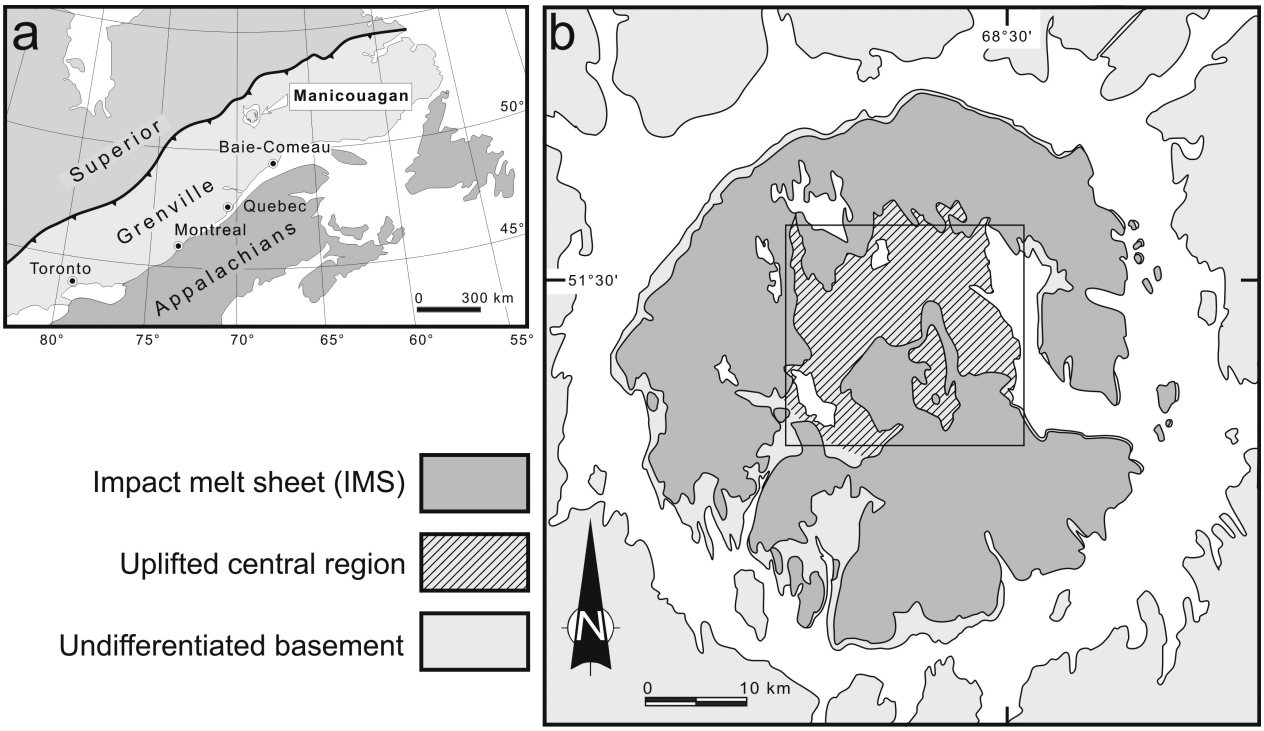

Fig. 1. a) Location of the Manicouagan impact structure within the Grenville Province of Canada. b) Simplified geology of the central part of the impact structure. The impact melt sheet (IMS) covers much of the central island. Boxed area detailed in Fig. 2a.

REGIONAL SETTING

The Manicouagan impact structure of Quebec, Canada (Fig. 1), is the fourth largest known crater on Earth; a rank held jointly with the Popigai impact structure of Siberia (Earth Impact Database 2008). The crater was formed at 214 Ma (Hodych and Dunning 1992) in predominantly Precambrian crystalline metamorphic rocks of the Grenville Province (Rivers 1997), possibly as part of a late Triassic multiple-impact event that involved at least three projectiles hitting Earth simultaneously (Spray et al. 1998; Carpozen and Gilder 2006). The target rocks at Manicouagan are characterized by 1700–1170 Ma anorthosite, mangerite, charnockite, granite (AMCG) suites and other associated igneous rocks with minor supracrustals, all of which were metamorphosed and deformed at amphibolite to granulite facies, and locally eclogite facies, conditions during the Grenville Orogeny (Cox et al. 1998; Indares et al. 1998). Anorthosite, including the centrally uplifted Mont de Babel and Maskelynite Peak (Fig. 2a), was most probably intruded into the charnockitic and granitic rocks as mid- to upper crust plutons. Both the anorthosite and granite/charnockite were subsequently intruded by gabbroic stocks, dykes and sills prior to, and possibly during, Grenville metamorphism. Thrusting and extensional collapse of the orogen facilitated rapid exhumation (within <100 Ma) after peak metamorphic conditions at 1100–1000 Ma (Indares et al. 1998). The target geology is thus dominated by late Mesoproterozoic Grenvillian orogenesis, but Archean and Paleoproterozoic signatures persist in certain units (Rivers 1997). In addition, there are sporadic outcrops of Trenton Group Ordovician limestones and shales that formed a thin cover to the metamorphic basement at the time of impact. Where these sedimentary rocks were directly juxtaposed with the impact melt sheet, they underwent pyrometamorphism, which is an indication of the once superheated state of the melt (Spray 2006).

The Manicouagan impact melt sheet (IMS) cooled to form a fine- to medium-grained igneous complex that covers much of the 55 km diameter central island (Currie 1972; Murtaugh 1976; Fig. 1b). The IMS has been reported as currently being up to 250 m thick, with an original pre-erosion thickness estimated at up to 400 m (Floran et al. 1978). The melt sheet, which has an average elevation above mean sea level (msl) of ~500 m, is underlain by shocked crystalline rocks, some of which protrude through the IMS as a central range of hills (up to 950 m above msl) that define the horseshoe-shaped uplift (Fig. 1b).

Since its inception in the late Triassic, the Manicouagan structure has undergone neither tectonothermal overprinting nor significant burial. It remains undeformed and well exposed, making it one of the better preserved of the larger terrestrial impact structures. The dominant post-impact modification process has been recent glaciation, which has removed the uppermost units of the structure such that no fallback has yet been found.

Over the last 15 years, an extensive drilling program carried out by mineral exploration companies has produced ~18 km of rock core from 38 locations on the island. Drilling has penetrated the IMS and underlying basement to provide information on melt sheet thickness variation and basement structure, and an unprecedented view of the inside of a large impact crater. Certain other terrestrial craters have been more extensively drilled, e.g., Popigai and Puchezh-Katunki in Russia (Earth Impact Database 2008), but much of those core collections have not been preserved (Koeberl and Milkereit 2007) and/or comprise shallower drill holes (typically <500 m). The drilling program at Manicouagan has focused on the center and western rim of the crater, and includes three holes in excess of 1.5 km deep (one of which is 1.8 km deep). In particular, drilling within the central region (holes M1—M9) since 2003 has revealed unexpectedly variable IMS compositions in hole M5 and a castellated topography to the IMS-basement contact. The relatively flat upper surface of the IMS thus belies highly variable footwall geometry. Here we report information from ten drill holes from the central region of the impact structure.

EVIDENCE FOR VARIABLE IMS-BASEMENT CONTACT MORPHOLOGY

A combination of drill core data, field mapping and surface sampling reveals the presence of a central, impact-melt filled trough, up to 1.5 km deep, surrounded by a 20 × 23 km horseshoe-shaped uplift, which includes Mont de Babel and Maskelynite Peak (Fig. 2a). The trough extends at least 8 km south from the flanks of Mont de Babel (Fig. 2b), as delineated by the presence of thick IMS sequences in drill holes M3, M5, and M6 (600, 1450, and 600 m melt thicknesses, respectively). The east-west dimensions are well constrained on the eastern edge of the trough by five drill holes, which contain little (<130 m; M4 and M7) or no IMS (M8 and M9) (Figs. 2d and 2e). The western boundary of the trough is less well defined, but two drill holes ~1.5 and 3 km west of M3 intersect 160 m and 60 m of IMS (M2 and M1, respectively, Fig. 2c), indicating an east-west trough dimension of ~3 km. Field work reveals that the central trough is open to the south (i.e., the trough was connected to the impact melt surrounding the horseshoe-shaped central uplift).

Abrupt changes (typically >1 km vertical offset) in the IMS-basement contact morphology within short lateral distances indicate steep-sided walls. For example, the anorthositic rocks of the southern edge of Mont de Babel are exposed within 1 km of drill hole M3, which intersects ~600 m of IMS before encountering basement lithologies (Fig. 2b). Figure 2d illustrates the marked change in depth to the IMS-basement contact over short lateral distances; from >1400 m depth in M5 (and >600 m in M5A, immediately adjacent to M5) to 130 m depth in M4 within a horizontal distance of ~800 m. This yields a depth to basement (H) to lateral separation of drill hole (W) ratio of >1, which indicates a slope angle of >45°. Holes M6 to M7 have a H/W of at least 0.5 (Fig. 2e).

The drill core information thus reveals variable melt sheet-basement morphology. Field mapping shows that the anorthositic gneisses that constitute Mont de Babel and Maskelynite Peak (Fig. 2) retain consistently trending foliations over distances of at least 10 km. Examination of the drill core confirms that the regional metamorphic textures of the rocks remain intact and unmodified by either gross thermal or structural overprinting, save for the localization of strain into discrete slip systems (faults). The submerged basement relief cannot, therefore, be attributed to plastic or fluid-like behavior of the target rocks. Moreover, it would be difficult to stabilize a 45° slope in material with low cohesion (e.g., rubble; Wu and Sun 2008).

Our interpretation of the data supports the presence of high-angle basement faults. The four geological cross sections (showing no vertical exaggeration) through the central region of the crater (Figs. 2a–e) depict the horseshoe-shaped central uplift comprising fault-bound blocks surrounding the central trough (Fig. 2a). Previous and ongoing field studies and mapping support this interpretation. For example, Murtaugh (1976) recognized a family of impact-related, steeply dipping lineaments striking at 70°, 110°, 160°, and 200° at Manicouagan. Faults with these trends occur in association with the central uplift, defining many of the horseshoe's straighter edges (Fig. 2a). These lineaments can be observed via NASA's Spaceborne Imaging Radar C/X-Band SAR (SRTM 2000), and they coincide with many of the fault systems in the cross sections (Figs. 2b–e). Notably, these faults do not breach the melt sheet, which indicates that they were active prior to IMS solidification. They do, however, define the margins of several faces of the uplift. It is not clear whether these fault systems represent reactivated pre-impact features, or whether they were created during the impact event. As is the case in other large impact structures (e.g., Sudbury; Spray et al. 2004), a combination of the two processes is likely.

TIMING RELATIONS: IMS FRACTIONATION AND COOLING

IMS Fractionation

In order to appraise any variations in IMS chemistry with IMS thickness we report major element analyses from five drill holes (Table 1). So as to avoid the effects of local contamination of the IMS by footwall heterogeneities and clasts, we do not report here on the impact-melt breccias that in places define the base of the IMS (e.g., in holes M3 and M5).

The results from the analysis of clast-free IMS from holes M2, 3, 4, and 6 are remarkably uniform (Fig. 3), aside

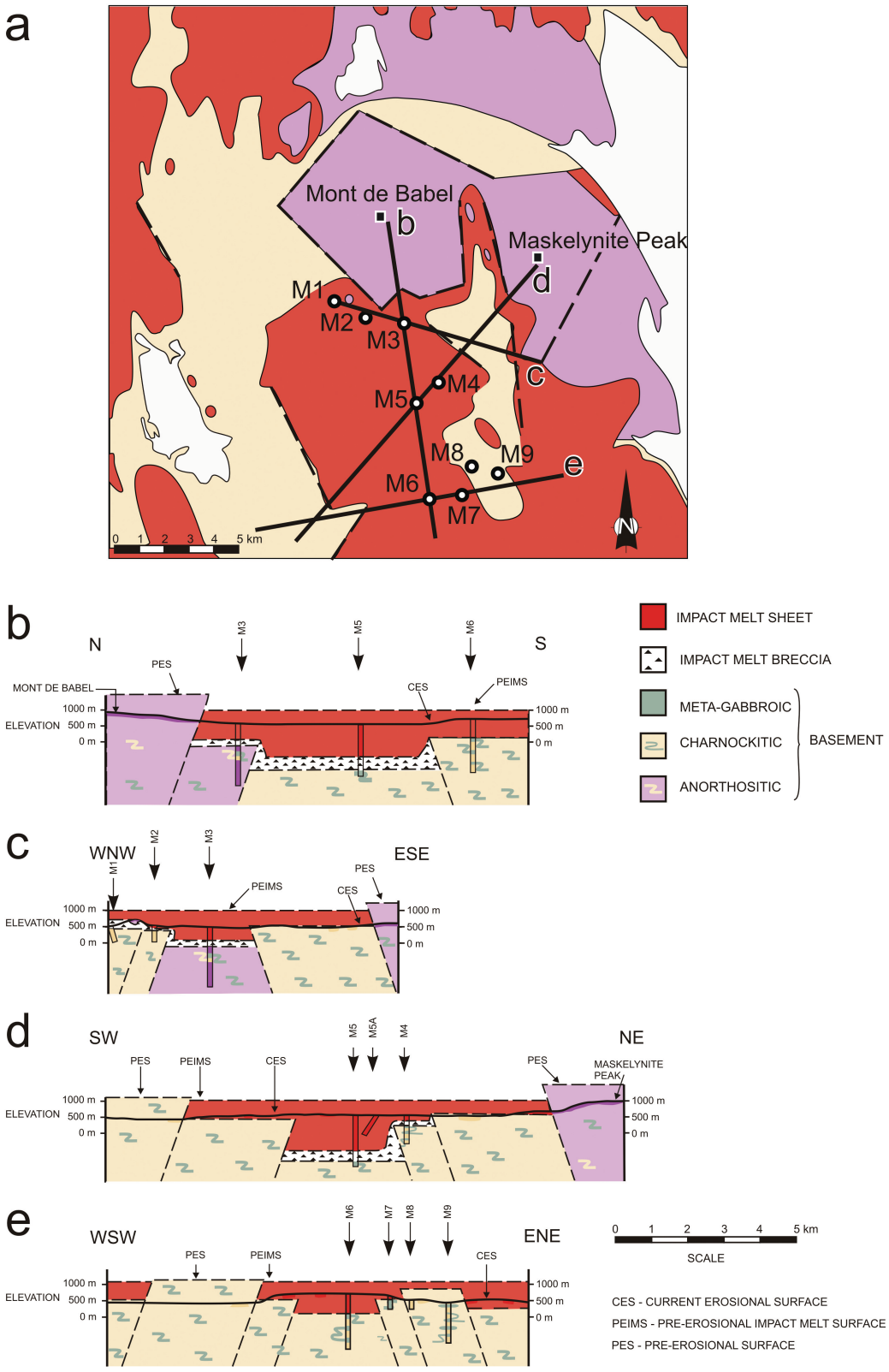

Fig. 2. a) Generalized geology of the central region of the impact structure (see Fig. 1b for context), showing drill hole locations (M1-9) and cross sections 2b, 2c, 2d, and 2e. Dashed lines in 2a indicate location of faults. Hole M5 (as shown in plan view in 2a) is immediately WSW of hole M5A (shown in cross section 2d). Impact melt sheet extent is derived from the work of Currie (1972), Murtaugh (1976), recent field studies and the new drill hole data. Exact fault dips are not known, but are relatively steep. See text for details.

Table 1. Major element oxide analyses and normative mineralogy of impact melt samples from drill holes M1–7 and previous work. UZ, TZ and LZ = Upper Zone, Transition Zone and Lower Zone of drill hole M5, respectively (this work). A: average from Floran et al. (1978). B: average from Currie (1972), as reported by Floran et al. (1978). Number of analyses given in brackets. nd: not determined. Analysis by X-ray fluorescence spectrometry.

wt%	M2–4 & 6 [25]	M5 UZ [15]	M5 TZ [5]	M5 LZ [11]	M5 average [31]	A [24]	B [26]
SiO_2	57.9	61.4	57.3	55.4	58.0	57.8	57.7
TiO_2	0.8	0.8	0.7	0.7	0.7	0.8	0.7
Al_2O_3	16.3	15.4	16.8	17.2	16.5	16.5	18.7
Fe_2O_3	6.7	6.0	6.8	7.4	6.8	6.0	5.8
MnO	0.1	0.1	0.1	0.1	0.1	0.1	0.1
MgO	3.7	2.4	4.1	4.5	3.6	3.5	3.5
CaO	5.9	3.7	6.3	7.0	5.6	5.9	5.8
Na_2O	3.8	3.6	3.6	3.7	3.6	3.8	4.0
K_2O	3.0	4.2	2.7	2.2	3.0	3.0	3.1
P_2O_5	0.2	0.2	0.2	0.2	0.2	0.2	nd
LOI	1.2	1.1	0.6	0.6	0.8	1.7	1.5
Total	99.6	98.9	99.2	99.0	98.9	99.3	100.9
CIPW norm (vol%)							
Quartz	5.8	12.1	5.7	2.8	7.3	6.4	3.3
Plagioclase	54.8	46.9	56.3	60.1	54.5	55.5	61.0
Orthoclase	20.0	27.6	18.0	14.8	20.0	20.0	20.2
Diopside	6.7	2.5	5.8	6.9	4.6	6.3	3.3
Hypersthene	10.6	8.9	12.1	13.3	11.6	9.7	10.7
Ilmenite	0.9	0.9	0.8	0.8	0.8	0.9	0.8
Magnetite	0.8	0.7	0.8	0.9	0.8	0.7	0.7
Apatite	0.4	0.4	0.4	0.4	0.4	0.4	nd

from a slight increase (~1 weight %) in SiO_2 (and K_2O) in the upper 200 m. The rocks show little or no evidence of fractionation or compositional layering. All analyses indicate a quartz monzodiorite composition. The average for these holes compares well with the results of previous work (columns A and B, Table 1, Fig. 3), especially that of Floran et al. (1978). The data of Currie (1972) shows minor differences in Al_2O_3 and Fe_2O_3 (total).

In contrast to the thinner IMS sections (<600 m thick), the most striking results come from drill hole M5, which comprises ~1100 m of clast-free IMS and another 350 m of impact-melt breccia (Figs. 2 and 3). Here the chemistry reveals segregation into two compositionally distinct layers separated by a transition zone, which together lie above the ~350 m thick impact-melt breccia (yielding a combined clast-bearing and clast-free IMS thickness of ~1500 m). The Lower Zone is ~450 m thick and is a monzodiorite (classification from Le Maitre 2002). The Transition Zone is ~180 m thick and is a quartz monzodiorite (similar to the average composition of the IMS intersected in the other holes). The Upper Zone is ~450 m thick and is a quartz monzonite. These chemical trends in M5 are reflected in the mineralogy, with plagioclase and pyroxenes decreasing in volume up-sequence, while quartz and potassium feldspar increase (see Table 1 norms). A more detailed appraisal of the chemical data will be presented elsewhere, but it is clear that, in contrast to the thinner IMS sections present in other drill holes, M5 was thick enough to facilitate the fractionation of the melt into three clast-free layers, presumably due to its larger volume and protracted cooling. Notably, the average composition of M5 is essentially the same as the average for the other drill holes (Table 1), which indicates that all were derived from a common, relatively well-mixed parent melt.

Critically, the Lower Zone monzodiorite layer of M5 is not manifest as a lower layer in any of the other drill holes, nor in any field samples collected. This reveals that the melt thickness in M5 is a primary feature and that the deep structure that hosts it was created prior to crystallization of the IMS. This concurs with the observation that most of the controlling faults do not propagate through the IMS, yet displace the underlying basement. This provides evidence for the basement topography being generated prior to solidification of the IMS.

IMS Cooling

Previous thermal modelling of the cooling of the IMS yielded estimates of 1600–5000 years for complete solidification of units <500 m, and <10,000 years for units ~1000 m thick (Oronato et al. 1978). Structural rigidity of the IMS could have been achieved significantly earlier if continuous three-dimensional

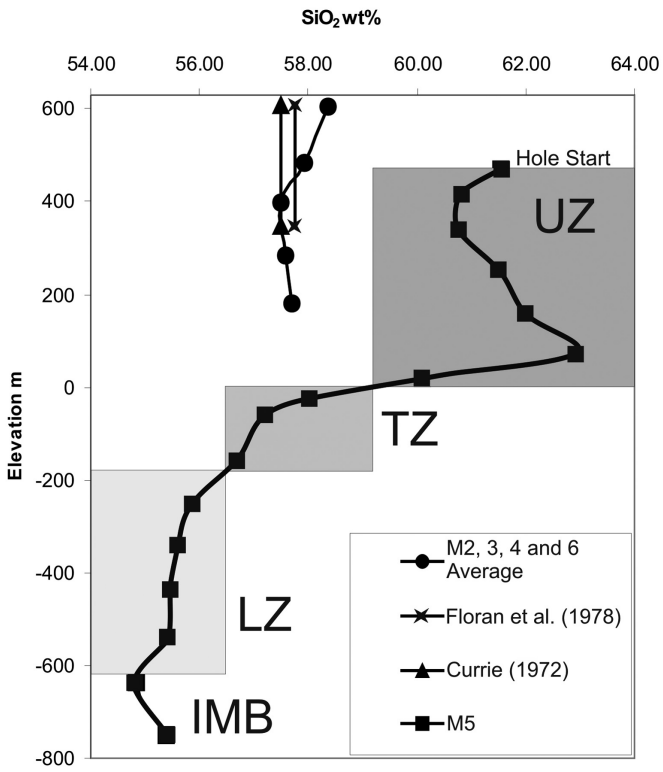

Fig. 3. SiO_2 versus elevation relative to mean sea level for IMS samples. Drill hole M5 is differentiated into three zones: LZ—Lower Zone, TZ—Transition Zone, UZ—Upper Zone. IMB = impact melt breccias. See text and Table 1 for details.

feldspar networks formed, as has been proposed for cooling intermediate and basaltic melt systems (Philpotts et al. 1998; Zeig and Marsh 2005). If so, the absence of deformation in the IMS mineral fabrics, as revealed by drill core and field samples, indicates that faulting occurred prior to IMS feldspar networking, probably within 1000 years of impact. This concurs with the presence of sanidine and uninverted pigeonite as high-temperature mineral phases in the IMS, both of which require rapid crystallization from temperatures above 700 °C (Deer et al. 1992). This is in accord with the fine- to medium-grained texture of the IMS mineral phases (i.e., coarse grain size is rare).

DISCUSSION

This work has presented evidence of variable IMS floor-basement relief beneath the center part of the Manicouagan impact structure. The thickest (~1500 m) known IMS section has fractionated into three distinct compositional layers (monzodiorite, quartz monzodiorite, quartz monzonite). The thinner (<600 m) IMS sections are relatively homogenous quartz monzodiorite. This shows that the basement relief was created before IMS solidification. This complies with the time scale of collapse and modification taking a few times $(D/g)^{½}$ (where D = crater diameter, g = surface gravity), which translates to ~3 minutes for a ~100 km diameter structure like Manicouagan (Melosh 1989).

Figure 4 illustrates four idealized scenarios for the formation of the central uplift and associated trough at Manicouagan. Figure 4a (i) depicts the central region undergoing inward and upward movement followed by collapse (Fig. 4a [ii]) facilitated by gross hydrodynamic behavior as favored by the modeling community using hydrocode simulations (e.g., Goldin et al. 2006). Figure 4b illustrates a horst and graben-type model for the formation of the structure. In this model the forces would be primarily extensional (centrifugal) leading to normal (extensional) faulting. Figure 4c describes a compressional (centripetal) regime whereby there is preferential uplift of the horst ring along steeply dipping reverse faults with the center remaining low. Figure 4d illustrates a two stage model for the formation of the central uplift and graben with initial compressional forces moving blocks inward and upward (Fig. 4d [i]). This is followed by collapse and downfaulting of the central area (Fig. 4d [ii]), whereby normal faulting accompanies down-dropping of the central core to form the graben, although the behavior of the underlying (deeper level) material is not known (i.e., how the uplift and down-drop were accommodated at depth). In smaller complex craters, there is good evidence for centripetal tectonics forming a central convergent zone (Fig. 4d [i]), such as for Upheaval Dome (Kenkmann et al. 2005) and Haughton (Osinski and Spray 2005). This mode of deformation typically evolves to divergent (centrifugal) motion for larger impact structures to eventually form a peak ring. However, Manicouagan does not appear to be a peak-ring basin in terms of its core structure.

Previous studies indicate that the change from a central peak to peak-ring basin occurs beyond a certain crater diameter, depending on the gravity field of the planetary body (e.g., >40 km for Venus, >25 km for Earth, and >175 km for the Moon; Wood and Head 1976; Pike 1985; Grieve and Cintala 1997). Moreover, the transition may occur via an intermediate multiple-peak stage (Melosh 1982; Alexopolous and McKinnon 1994). This should place Manicouagan as a peak-ring basin (Grieve and Head 1983). However, for a collapsed crater rim to rim diameter of ~90 km for Manicouagan, the diameter of the horseshoe-shaped uplift (23 km) does not comply with the generally accepted relationship between peak-ring diameter and crater rim diameter: $D_{pr} = 0.5\ D$ (Wood and Head 1976), but more closely with central peak diameter to crater rim diameter $D_{cp} = 0.22\ D$ (Pike 1985).

The presence of a graben within the horseshoe's core suggests that Manicouagan could be a central floor pit variant of a central peak basin (Barlow and Azate 2008). However, central pit craters are common in ice-rich targets, such as Mars, Ganymede and Callisto, but are as yet unknown on volatile-poor bodies like the Moon and Mercury. Given the low-porosity, hard rock target at Manicouagan, formation of a

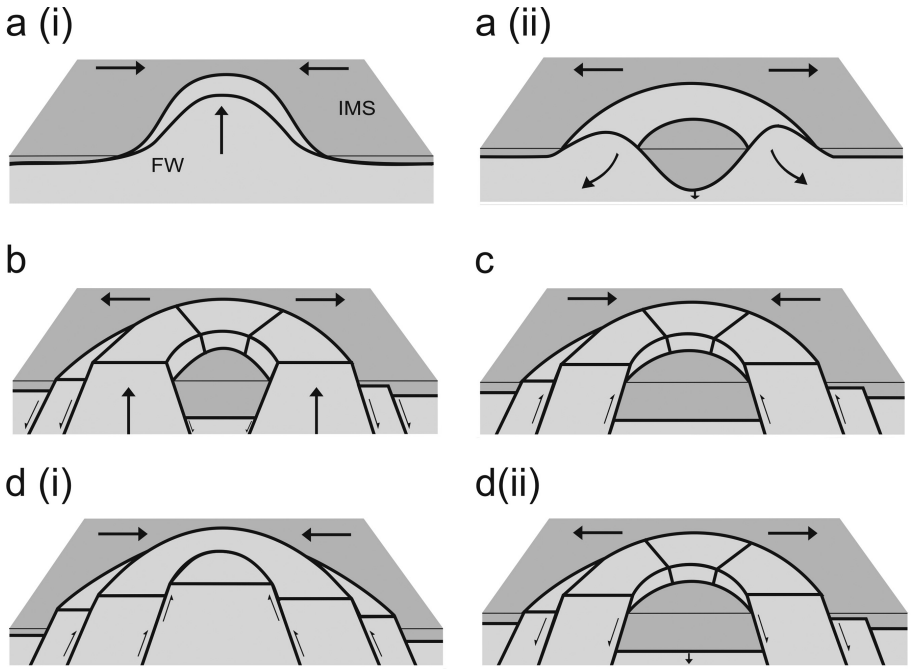

Fig. 4. Simplified cross sections of models for central peak formation at Manicouagan. IMS = impact melt sheet; FW = footwall. a) Hydrodynamic behavior of target; (i) uplift (rebound) to form central peak (centripetal movement) followed by (ii) collapse to form a central peak annulus (centrifugal movement). b) Uplift of main blocks (horsts), with associated down-dropping of center (graben) and horst outer margins (extensional). c) Inward migration of convergent fault-bound units (possibly listric at depth). d) (i) initial convergent tectonics with uplift followed by (ii) central peak core collapse to form a graben.

pit by volatile release is considered unlikely. As yet, we are unclear as to exactly how the graben (central pit-like) structure formed at Manicouagan (Fig. 4). We favor formation by annular horst-graben development (Fig. 4b), convergent tectonics generating a partial ring (Fig. 4c), or central uplift core collapse (Fig. 4d).

In terms of morphological comparisons with other craters, Manicouagan shows similarities with the lunar far side crater King (75 km diameter), which exhibits a distinctive claw-shaped central peak complex (e.g., Heather and Dunkin 2003). Comparisons can also be made with the lunar craters Tycho (85 km diameter), Copernicus (93 km diameter), Arzachel (96 km) and Gassendi (110 km). These are all central peak basins and are also comparable in diameter, which is problematic given the different gravity fields of the Moon and Earth (i.e., comparable morphologies should be reached at somewhat larger diameters on the Moon given 1/g scaling laws).

Fault offsets within the central basement region at Manicouagan range from 250 m to over 1000 m (Fig. 2). Field and geophysical evidence reveals that the central uplift has been elevated at least 10 km from the floor of the transient cavity (Grieve and Pilkington 1996). For this to take place when the overlying IMS was still liquid, these movements must have occurred in single or multiple mega-slip events. The coherent nature of the basement lithologies, as revealed in drill core and in the field, combined with high-angle basement relief, renders a purely hydrodynamic model implausible. Faulting has previously been proposed for sidewall slumping (Spray 1997) and ring formation in impact basins beyond the transient cavity (Spray and Thompson 1995; Melosh 2005). Here we have extended the role of large-displacement faults and heterogeneous (brittle) strain conditions to central peak—trough formation during the modification stage of the cratering process in a relatively large terrestrial complex impact structure.

SUMMARY

1. Recent drilling operations in the central region of the 214 Ma Manicouagan impact structure have revealed highly variable morphology between the impact melt sheet (IMS) and underlying basement rocks of the Grenville Province.
2. The thickest melt sheet unit intersected (via drill hole M5) reveals a fractionated three-layer IMS, with the lowermost layer being a monzodiorite. This lower layer is not present in the lower levels of any of the thinner IMS units, which instead possess a more homogeneous (unfractionated) quartz monzodiorite composition. This places important constraints on the timing of deformation associated with the formation of the central peak-trough system. Faulting in the basement must have been active during the modification stage, prior to solidification of the IMS, such that the present thickness variation in the IMS is a primary feature (i.e., although

minor fault adjustments may have occurred well after impact, most displacement took place during the modification stage prior to IMS solidification). This complies with the known collapse times for the modification stage of the impact process (i.e., within minutes of impact for a crater of Manicouagan's diameter).

3. The variable IMS-basement morphology, with some basement slopes being 45° or steeper, favors the presence of high-angle fault systems. Many of the faults, as inferred from drill core data, link to lineament trends in the central region of the impact crater that define the margins of the horseshoe-shaped annulus (central uplift) and related discontinuities. Total displacement on these faults is 100s to 1000s of meters.
4. The continuity of Grenvillian regional metamorphic fabrics within the central uplift lithologies, as observed both in the field and in drill core, shows that the rocks behaved in a coherent manner and were never fluid-like during the impact event.
5. The nature of the central uplift at Manicouagan is puzzling. Based on the development of an outermost ring at ~150 km diameter and a collapsed transient cavity ring at ~90 km, previous studies have suggested that Manicouagan is a peak-ring basin (Grieve and Head 1983), or is transitional to a multi-ring basin (Floran and Dence 1976). This work indicates that Manicouagan is a central peak basin with rings, which does not appear to fit with current complex crater scaling models. The classification of impact craters is based primarily on morphological surface observations from the Moon and, to a lesser extent, other planets. For example, a complex central peak or peak-ring crater is defined as having the central peak or peak-ring rising through and breaching the IMS. This classification does not take into consideration what has occurred beneath the melt sheet. Drilling at Manicouagan facilitates observation of the third dimension and reveals a highly variable basement structure concealed beneath the IMS. In addition to the uplifted anorthositic massifs Mont de Babel and Maskelynite Peak, which rose through the IMS, significant uplift (100s of m) of basement occurred without ever having breached the melt sheet.
6. Along with Sudbury, Manicouagan is only the second impact crater so far known to unequivocally exhibit impact melt sheet fractionation. Morokweng in South Africa may constitute a third example, where granophyre and norite have been identified in 870 m of impact melt in drill hole M3 (Hart et al. 2002). At Manicouagan, the fractionated unit occurs in a graben or trough-like structure. This work shows that the contact between an impact melt sheet and its footwall may possess a highly variable morphology, which needs to be accommodated in our models of impact crater formation.

Acknowledgments—This Manicouagan Impact Research Program is supported by the Canada Research Chairs program, the Canadian Space Agency, the Natural Sciences and Engineering Research Council of Canada (NSERC), the University of New Brunswick and Manicouagan Minerals Inc. (MMI). We are particularly grateful to Constantine Salamis and Rod Thomas of MMI for logistical support in 2006. We thank Robbie Herrick for constructive comments on an earlier version of the manuscript and especially Mike Dence for fruitful discussions and thought-provoking reviews. Planetary and Space Science Centre Contribution 60.

Editorial Handling—Dr. Robert Herrick

REFERENCES

Alexopolous J. S. and McKinnon W. B. 1994. Large impact craters and basins on Venus, with implications for ring mechanics on the terrestrial planets. In *Large meteorite impacts and planetary evolution I*, edited by Dressler B. O., Grieve R. A. F., and Sharpton V. L. GSA Special Paper 293. Washington, D.C.: Geological Society of America. pp. 29–50.

Barlow N. G. and Azate N. 2008. Central pit craters on Mars and Ganymede: Characteristics, distributions, and implications for formation models (abstract #3071). Large Meteorite Impacts and Planetary Evolution IV.

Carpozen L. and Gilder S. A. 2006. Evidence for coeval Late Triassic terrestrial impacts from the Rochechouart (France) meteorite crater. *Geophysical Research Letters* 33:L19308, doi:10.1029/2006/GL027356.

Cox R., Dunning G. R., and Indares A. 1998 Petrology and U-Pb geochronology of mafic, high pressure metamorphic coronites from the Tshenukutish domain, eastern Grenville Province. *Precambrian Research* 90:59–83.

Crawford D. A. and Schultz P. H. 1999. Electromagnetic properties of impact-generated plasma, vapor and debris. *International Journal of Impact Engineering* 23:169–180.

Currie K. L. 1972. Geology and petrology of the Manicouagan resurgent caldera, Quebec. *Geological Survey of Canada Bulletin* 198. 153 p.

Deer W. A., Howie R. A., and Zussman J. 1992. *An introduction to the rock-forming minerals*. London: Longman Scientific. 696 p.

Dressler B. O. and Reimold W. U. 2001. Terrestrial impact melt rocks and glasses. *Earth Science Reviews* 56:205–284.

Earth Impact Database. 2008. <http://www.unb.ca/passc/ImpactDatabase>. Accessed: 10 September 2008.

Floran R. J. and Dence M. R. 1976. Morphology of the Manicouagan ring-structure, Quebec, and some comparisons with lunar basins and craters. Proceedings, 7th Lunar Science Conference. pp. 2845–2865.

Floran R. J., Grieve R. A. F., Phinney W. C., Warner J. L., Simonds C. H., Blanchard D. P., and Dence M. R. 1978. Manicouagan impact melt, Quebec, 1, stratigraphy, petrology and chemistry. *Journal of Geophysical Research* 83:2737–2759.

French B. M. 1998. *Traces of catastrophe*. LPI Contribution 954. Houston, Texas: Lunar and Planetary Institute. 120 p.

Goldin T. J., Wünnemann K., Melosh H. J., and Collins G. S. 2006. Hydrocode modeling of the Sierra Madera impact structure. *Meteoritics & Planetary Science* 41:1947–1958.

Grieve R. A. F. and Cintala M. J. 1997. Planetary differences in impact cratering. *Advances in Space Science* 20:1551–1560.

Grieve R. A. F. and Head J. W. 1983. The Manicouagan impact structure: An analysis of its original dimensions and form. *Journal of Geophysical Research* 88:A807–A818.

Grieve R. A. F. and Pilkington M. 1996. The signature of terrestrial impacts. *AGSO Journal of Australian Geology and Geophysics* 16:399–420.

Hart R. J., Cloete M., McDonald I., Carlson R. W., and Andreoli M. A. G. 2002. Siderophile-rich inclusions from the Morokweng impact melt sheet, South Africa: Possible fragments of a chondritic meteorite. *Earth and Planetary Science Letters* 198: 49–62.

Heather D. J. and Dunkin S. K. 2003. Geology and stratigraphy of King crater, lunar farside. *Icarus* 163:307–329.

Hodych J. P. and Dunning G. R. 1992. Did the Manicouagan impact trigger end-of-Triassic mass extinction? *Geology* 20:51–54.

Indares A., Dunning G., Cox R., Gale D., and Connelly J. 1998. High-PT rocks from the base of thick continental crust: Geology and age constraints from the Manicouagan Imbricate Zone, eastern Grenville Province. *Tectonics* 17:426–440.

Kenkmann T., Jahn A., Scherler D., and Ivanov B. A. 2005. Structure and formation of a central uplift: A case study at the Upheaval Dome impact crater, Utah. In *Large meteorite impacts III*, edited by Kenkmann T., Hörz F., and Deutsch A. GSA Special Paper 384. Washington, D.C.: Geological Society of America. pp. 85–115.

Koeberl C. and Milkereit B. 2007. Continental drilling and the study of impact craters and processes—An ICDP perspective. In *Continental scientific drilling*, edited by Harms U., Koeberl C., and Zoback M. D. Berlin: Springer. pp. 95–161.

Le Maitre R. W., ed. 2002. *Igneous rocks. A classification and glossary of terms*. Cambridge, UK: Cambridge University Press. 236 p.

Melosh H. J. 1982. A schematic model for crater modification by gravity. *Journal of Geophysical Research* 87:371–380.

Melosh H. J. 1989. *Impact cratering: A geologic process*. New York: Oxford University Press. 245 p.

Melosh H. J. 2005. The mechanics of pseudotachylite formation in impact events. In *Impact tectonics*, edited by Koeberl C. and Henkel H. New York: Springer. pp. 55–80.

Murtaugh J. C. 1976. Manicouagan impact structure. Quebec Department of Natural Resources, Open-File Report DPV-432. 180 p.

Onorato P. I. K., Uhlmann D. R., and Simonds C. H. 1978. The thermal history of the Manicouagan impact melt sheet, Quebec. *Journal of Geophysical Research* 83:2789–2798.

Osinski G. R. and Spray J. G. 2005. Tectonics of complex crater formation as revealed by the Haughton impact structure, Devon Island, Canadian High Arctic. *Meteoritics & Planetary Science* 40:1813–1834.

Philpotts A. R., Jianyang S., and Brustman C. 1998. Role of plagioclase crystal chains in the differentiation of partly crystallized basaltic magma. *Nature* 395:343–346.

Pike R. J. 1985. Some morphologic systematics of complex impact structures. *Meteoritics* 20:49–68.

Rivers T. 1997. Lithotectonic elements of the Grenville province: Review and tectonic implications. *Precambrian Research* 86: 117–154.

Spray J. G. 1997. Superfaults. *Geology* 25:579–582.

Spray J. G. 2006. Ultrametamorphism of impure carbonates beneath the Manicouagan impact melt sheet: Evidence for superheating (abstract #2385). 37th Lunar and Planetary Science Conference. CD-ROM.

Spray J. G., Kelley S. P., and Rowley D. B. 1998. Evidence for a late Triassic multiple impact event on Earth. *Nature* 392:171–173.

Spray J. G. and Thompson L. M. 1995. Friction melt distribution in a multi-ring impact basin. *Nature* 373:130–132.

Spray J. G., Butler H. R., and Thompson L. M. 2004. Tectonic influences on the morphometry of the Sudbury impact structure: Implications for terrestrial cratering and modeling. *Meteoritics & Planetary Science* 39:287–301.

SRTM. 2000. <http://photojournal.jpl.nasa.gov/tiff/PIA03385.tif>. NASA Shuttle Radar Topographic Mission.

Wood C. A. and Head J. W. 1976. Comparison of impact basins on Mercury, Mars and the Moon. Proceedings, 7th Lunar Science Conference. pp. 3629–3651.

Wu A. and Sun Y. 2008. *Granular dynamic theory and its applications*. New York: Springer. 300 p.

Zeig M. J. and Marsh B. D. 2005. The Sudbury igneous complex: Viscous emulsion differentiation of a superheated impact melt. *Geological Society of America Bulletin* 117:1427–1450.